

# Accurate Determination of Blackbody Radiation Shifts in a Strontium Molecular Lattice Clock

B. Iritani<sup>1,\*</sup>, E. Tiberi<sup>1,\*</sup>, W. Skomorowski<sup>2</sup>, R. Moszynski<sup>3</sup>, M. Borkowski<sup>1,4,5,†</sup> and T. Zelevinsky<sup>1,‡</sup>

<sup>1</sup>Department of Physics, Columbia University, 538 West 120th Street, New York, NY 10027-5255, USA

<sup>2</sup>Centre of New Technologies, University of Warsaw, Banacha 2c, 02-097 Warsaw, Poland

<sup>3</sup>Quantum Chemistry Laboratory, Department of Chemistry,  
University of Warsaw, Pasteura 1, 02-093 Warsaw, Poland

<sup>4</sup>Van der Waals-Zeeman Institute, Institute of Physics, University of Amsterdam,  
Science Park 904, 1098 XH Amsterdam, The Netherlands

<sup>5</sup>Institute of Physics, Faculty of Physics, Astronomy and Informatics,  
Nicolaus Copernicus University, Grudziadzka 5, 87-100 Torun, Poland

(Dated: November 3, 2023)

Molecular lattice clocks enable the search for new physics, such as fifth forces or temporal variations of fundamental constants, in a manner complementary to atomic clocks. Blackbody radiation (BBR) is a major contributor to the systematic error budget of conventional atomic clocks and is notoriously difficult to characterize and control. Here, we combine infrared Stark-shift spectroscopy in a molecular lattice clock and modern quantum chemistry methods to characterize the polarizabilities of the  $\text{Sr}_2$  molecule from dc to infrared. Using this description, we determine the static and dynamic blackbody radiation shifts for all possible vibrational clock transitions to the  $10^{-16}$  level. This constitutes an important step towards mHz-level molecular spectroscopy in  $\text{Sr}_2$ , and provides a framework for evaluating BBR shifts in other homonuclear molecules.

Frequency standards are the cornerstone of precision measurement. Among them, optical atomic clocks set records in both precision and accuracy, and are poised to redefine the second [1–7]. Complementing these atomic systems there is a growing interest in precision measurements with molecules [8–12]. The simple structure of homonuclear diatoms, such as  $\text{Sr}_2$ , makes them ideal testbeds to probe new avenues for fundamental physics, including searches for corrections to gravity at short distances [13–16] and tests of the temporal variation of fundamental constants [12, 17–26]. As such, there is interest in improving techniques for molecular spectroscopy. Even for ultra-precise atomic clocks, the blackbody radiation (BBR) shift remains a primary contribution to the overall uncertainty of the clock measurement [3, 4, 27–32], and is notoriously difficult to control and characterize [33–35]. State-of-the-art evaluations of BBR shift rely on accurate measurements of the differential dc polarizability of the clock states in conjunction with robust modeling of dynamic contributions [36–40].

In our previous work, we demonstrated record precision and accuracy for a molecular lattice clock by measuring a 32 THz transition between two vibrational levels in ultracold  $\text{Sr}_2$  molecules, reaching a  $4.6 \times 10^{-14}$  systematic uncertainty [41]. Estimates of the BBR contribution to this uncertainty relied on preliminary theoretical modelling of polarizabilities that lacked experimental verification. In this Letter, we determine room-temperature BBR shifts for our molecular clock to the  $10^{-16}$  level. To do so, we employ modern quantum chemistry methods to determine the differential polarizabilities for all vibrational clock transitions. We then verify our theory directly by measuring ac Stark shifts induced by a  $1.95 \mu\text{m}$  laser for a wide variety of molecular clock transitions (Fig. 1). Given this combined experimental and theoretical picture, we develop a complete description of the BBR effect. Below, we describe a robust theoretical model, experimentally

validate and extend this model to other relevant wavelengths, and determine the BBR shift for all vibrational levels within the ground-state electronic potential of  ${}^{88}\text{Sr}_2$  molecules.

The experimental sequence closely follows that of our previous works [9, 41–43]. Briefly, a  $2\mu\text{K}$  sample of ultracold strontium atoms is trapped in a one-dimensional horizontal optical lattice in the near-infrared. We form weakly bound molecules via a photoassociation pulse tuned to the  $-353\text{-MHz } 1_u$  resonance [44]. This bound state predominantly decays to a pair of rotational  $J = 0, 2$  states of the least bound vibrational state,  $v' = 62$ , in the ground-state potential. For a given measurement, we apply a two-photon Raman pulse to probe the selected clock transition. We detect the number of remaining  $v' = 62$  molecules by photodissociating them near the  ${}^1\text{S}_0 + {}^3\text{P}_1$  threshold [45] and counting the recovered atoms. Unless otherwise specified, we always refer to rotationless  $J = 0$  states in the electronic ground-state potential, and list the lower energy state first for a given transition, regardless of where the molecular population is initialized.

Our clock spectroscopy relies on narrow-linewidth Raman transitions between the least bound  $v' = 62$  vibrational state and a selection of more deeply bound vibrational states  $v$  of the  $\text{Sr}_2$  molecule [shown for  $0 \leftrightarrow 62$  in Fig. 1(a)]. We address each of these transitions via intermediate states  $v''$  in the electronically excited  $(1)0_u^+$  potential. The vibrational splittings are determined by the difference in the pump ( $v' \rightarrow v''$ ) and anti-Stokes ( $v'' \rightarrow v$ ) laser frequencies. We select intermediate states with favorable Franck-Condon factors for the pump and anti-Stokes transitions for each interrogated pair of clock states (Table I). In order to address clock states throughout the potential well, we use 3 different intermediate states in the excited  $(1)0_u^+$  potential:  $v'' = 11$  [at  $-57\,084\,156.51(12)$  MHz from the  ${}^1\text{S}_0 + {}^3\text{P}_1$  threshold],  $v'' = 15$  [at  $-48\,855\,512.13(18)$  MHz], and  $v'' = 16$  [at  $-47\,036\,433.95(23)$  MHz]. The selection of intermediate

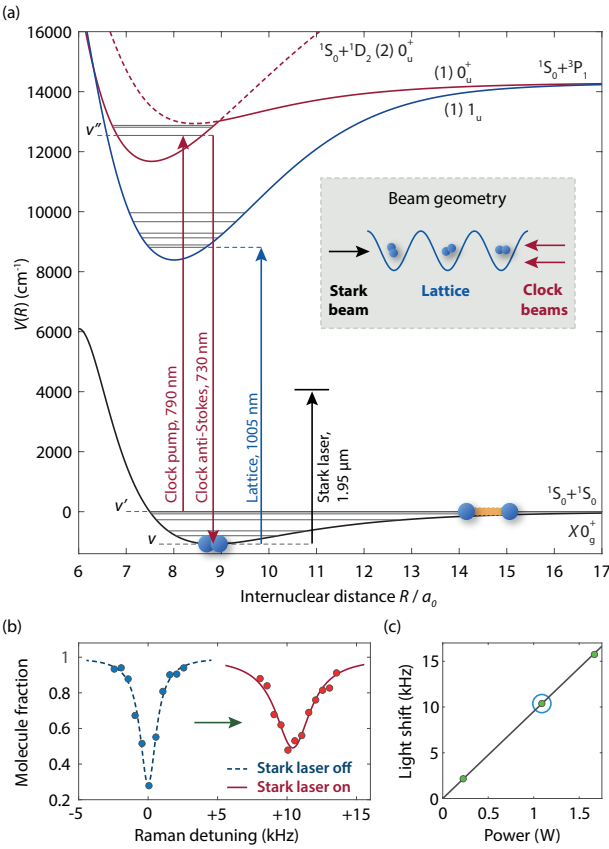


FIG. 1. Stark shift spectroscopy in a  $\text{Sr}_2$  molecular clock on the example  $0 \leftrightarrow 62$  transition. (a) Our molecular clock relies on narrow two-photon Raman transition via an intermediate state in the  $(1) 0_u^+$  (red arrows) in a magic lattice that couples the deeply-bound clock state  $v$  to an excited  $(1) 1_u$  state (blue arrow). (b) We induce Stark shifts to probe differential polarizabilities of ground ro-vibrational states with  $1.95 \mu\text{m}$  light. (c) Example light shift measurement. The encircled data point corresponds to the spectrum shown in (b).

states is a balancing act between available lasers and transition strengths, and requires several diode lasers in the 727–735 nm and 760–800 nm wavelength ranges.

We initially locate the target vibrational states  $v$  using Autler-Townes spectroscopy: we first induce molecular loss with the pump laser, and then scan the anti-Stokes laser until the line is split into a doublet [43, 46–50]. While high-precision absolute determinations of these binding energies are beyond the scope of this Letter, we list the vibrational splittings  $f_{v \leftrightarrow v'}$  to  $\sim 100$  kHz precision (Table I). We estimate the uncertainty as fully dominated by light shifts (Supplemental Material).

We employ several strategies to achieve 1 kHz spectroscopic resolution, which enables us to determine ac Stark shifts to  $\sim 150$  Hz using Lorentzian fits (Supplemental Material). After initially locating the transitions, we switch to a Raman configuration by detuning  $+30$  MHz from the intermediate resonance in order to narrow down our transition linewidth. We stabilize the pump laser to a high finesse

$(> 3 \times 10^5)$  cavity using a Pound-Drever-Hall lock [52, 53], which in turn provides a stable reference for the repetition rate of an optical frequency comb. We then lock our anti-Stokes clock laser to the frequency comb. This locking scheme ensures the stability of the frequency difference between the two Raman lasers. In addition to stabilizing our clock lasers, we rely on magic-wavelength trapping to reduce inhomogenous broadening. Our method for magic trapping utilizes polarizability crossings generated by the dispersive behavior of the target state polarizability near transitions to the electronically excited  $(1) 1_u$  potential [9]. We select  $(1) 1_u$  states such that the line strength  $S$  [42] is greater than  $\sim 10^{-5} (ea_0)^2$  (here  $e$  is the electron charge,  $a_0$  is the Bohr radius). Large line strengths correspond to large magic detunings, allowing molecular lifetimes of a few ms, and Fourier-limited linewidths of 1 kHz or better. Our lattice laser is wavemeter-locked to  $\sim 30$  MHz precision.

To determine differential polarizabilities we induce ac Stark shifts on these clock transitions using an additional  $1.95 \mu\text{m}$  laser. We typically observe ac Stark shifts of up to 20 kHz [as shown for  $0 \leftrightarrow 62$  in Fig. 1(b)]. We measure ac Stark shifts of each transition as a function of  $1.95 \mu\text{m}$  laser power [Fig. 1(c)] relative to the  $27 \leftrightarrow 62$  transition. We do not observe any significant hyperpolarizability [41] and therefore we fit a simple proportion. To determine the differential polarizability, we need to adequately characterize the intensity of the  $1.95\text{-}\mu\text{m}$  light at our molecules. We calibrate the intensity of the  $1.95\text{-}\mu\text{m}$  light by comparing the ac Stark shift of the  $27 \leftrightarrow 62$  transition to that of the  $\Delta m = 0$  component of atomic intercombination  $^1\text{S}_0 \rightarrow ^3\text{P}_1$  transition with a differential polarizability of  $+326.2(3.6)$  a.u. [54]. For our maximum power of  $1.7$  W, we have an intensity of  $6.8 \text{ kW/cm}^2$ . For most transitions, this scheme allows us to determine the differential polarizabilities to 5% as listed in Table I and shown in Fig. 2.

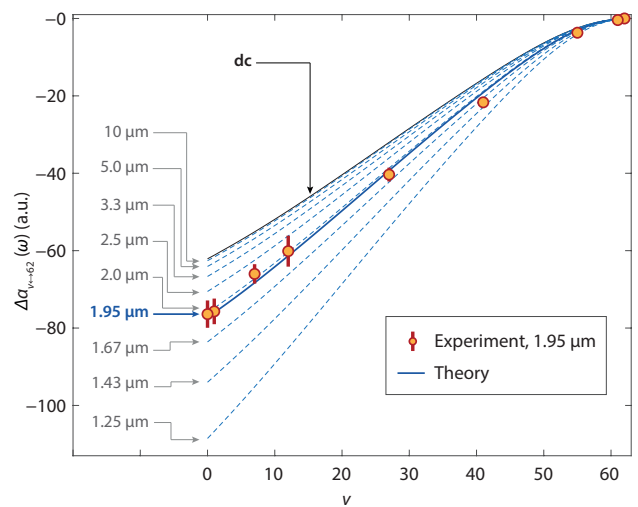


FIG. 2. Differential polarizability with respect to the least-bound  $v = 62$  state in ground state  $\text{Sr}_2$ . Points denote experimentally measured ac polarizabilities at  $\lambda = 1.95 \mu\text{m}$ . Lines are *ab initio* polarizabilities from dc to  $\lambda = 1.25 \mu\text{m}$ .

TABLE I. Bound states of the  $^{88}\text{Sr}_2$  molecule investigated in this work. The initial molecular state is always the rotationless near-threshold  $v' = 62$  level. Here  $v$  denotes the vibrational quantum number of the target bound state in the electronic  $^1\text{S}_0 + ^1\text{S}_0 0_g^+$  ground state and  $\lambda_{\text{magic}}$  is the magic wavelength. The differential polarizabilities are expressed in atomic units of  $e^2 a_0^2 / E_h$ , where  $e$  is the electron charge,  $a_0$  is the Bohr radius and  $E_h$  is the Hartree energy [51]. The error bars on theoretical polarizabilities stem from comparison to experiment.

Clock transitions			Differential polarizability $\alpha_{v \leftrightarrow v'}(\omega)$ (a.u.)							
$X\ 0_g^+$	$v \leftrightarrow v'$	$v''$	$f_{v \leftrightarrow v'}$ (MHz)	$\tilde{R}_v$ (a.u.)	$\lambda_{\text{magic}}$ (nm)	Exp. (1.95 $\mu\text{m}$ )	Th. (1.95 $\mu\text{m}$ )	Th. (dc)	$\Delta f_{v \leftrightarrow v'}$ (Hz)	
61 $\leftrightarrow$ 62	15		1263.673 58(20) [45]		43.6	–	-0.41(0.52)	-0.1326(35)	-0.1080(28)	+9.32(25) $\times 10^{-4}$
55 $\leftrightarrow$ 62	15		108 214.221(10)		21.6	–	-3.68(0.38)	-2.985(78)	-2.429(63)	+0.020 99(56)
41 $\leftrightarrow$ 62	11		2 177 876.735(81)		13.6	996.4379(10)	-21.67(0.88)	-19.10(50)	-15.60(41)	+0.134 9(37)
27 $\leftrightarrow$ 62	11		8 075 406.280(18)		11.1	1006.5787(10)	-40.4(1.8)	-39.3(1.0)	-31.99(84)	+0.276 8(75)
12 $\leftrightarrow$ 62	16		19 176 451.651(35)		9.62	1007.7634(10)	-60.1(4.0)	-61.3(1.6)	-49.7(1.3)	+0.430(12)
7 $\leftrightarrow$ 62	15		24 031 492.422(24)		9.27	1007.1334(10)	-66.0(2.5)	-68.3(1.8)	-55.1(1.4)	+0.477(13)
1 $\leftrightarrow$ 62	11		30 640 159.753(75)		8.91	1016.9714(10)	-75.7(3.3)	-76.0(2.0)	-61.1(1.6)	+0.529(15)
0 $\leftrightarrow$ 62	11	31 825 183.207 5928(51) [41]		8.86	1004.7720(10)		-76.4(3.6)	-77.2(2.0)	-62.1(1.7)	+0.538(15)

Any thermal shifts stemming from our 5- $\mu\text{K}$  sample [55] are negligible (Supplemental Material).

To calculate the BBR shifts we need a model of the differential polarizabilities at all wavelengths from dc to infrared. The overwhelming majority of the BBR spectrum falls below 2  $\mu\text{m}$ . While we cannot experimentally probe this entire range of wavelengths, we can leverage close agreement between theory and experiment at 1.95  $\mu\text{m}$  and extend theoretical models to provide a full description of the BBR shift. We use modern quantum chemistry methods to calculate the differential po-

larizabilities for all molecular clock transitions in two steps: first, we calculate *ab initio* electronic polarizabilities of the strontium dimer as a function of internuclear distance  $R$ , and second, we obtain the polarizability for each vibrational level as an average of the electronic polarizability over the vibrational wavefunction.

In homonuclear molecules only electronic transitions contribute to polarizabilities and BBR shifts. To calculate the electronic polarizability, we employ the approach based on asymmetric analytical derivative of the coupled-cluster energy with single and double excitations (CCSD) [58], as implemented in the Q-Chem 5 package [59]. We use the ECP28MDF pseudopotential together with its dedicated valence basis set [60]. For any given lattice light frequency  $\omega$ , we first calculate the interaction-induced polarizability of  $\text{Sr}_2$  molecules,  $\alpha_{ij}^{\text{int}}(\omega; R) = \alpha_{ij}(\omega; R) - 2\alpha_{\text{atom}}(\omega)$ , where  $\alpha_{ij}(\omega)$  are tensor components of the total molecular polarizability and  $\alpha_{\text{atom}}(\omega)$  is the atomic polarizability at frequency  $\omega$ . Since we are working only with isotropic  $J = 0$  states, we take the trace polarizability  $\alpha^{\text{int}}(\omega; R) = [\alpha_{zz}^{\text{int}}(\omega; R) + 2\alpha_{xx}^{\text{int}}(\omega; R)]/3$  [61, 62]. We extend the model for large  $R$  using a fitted long-range form  $\alpha^{\text{int}}(\omega; R) \sim A_6(\omega)R^{-6} + A_8(\omega)R^{-8} + A_{10}(\omega)R^{-10}$  [63]. Figure 3 shows the isotropic component  $\alpha^{\text{int}}(\omega; R)$  at 1.95  $\mu\text{m}$  as a function of  $R$ .

In the second step, we calculate the polarizability of each vibrational level  $v$  by averaging the electronic polarizability  $\alpha^{\text{int}}(R)$  over the level's vibrational wavefunction  $\Psi_v(R)$ :

$$\alpha_v^{\text{int}}(\omega) = \int_0^{\infty} |\Psi_v(R)|^2 \alpha^{\text{int}}(\omega; R) dR \quad (1)$$

where the differential polarizability for a transition  $v \leftrightarrow v'$  is

$$\Delta\alpha_{v \leftrightarrow v'}(\omega) = \alpha_{v'}^{\text{int}}(\omega) - \alpha_v^{\text{int}}(\omega). \quad (2)$$

We obtain the vibrational wavefunctions by solving the Schrödinger equation,  $[-(\hbar^2/2\mu)(d^2/dR^2) + V(R)]\Psi_v(R) = E_v\Psi_v(R)$ , using a discrete variable representation (DVR) [64, 65]. We use an empirical molecular potential  $V(R)$  [66]; the

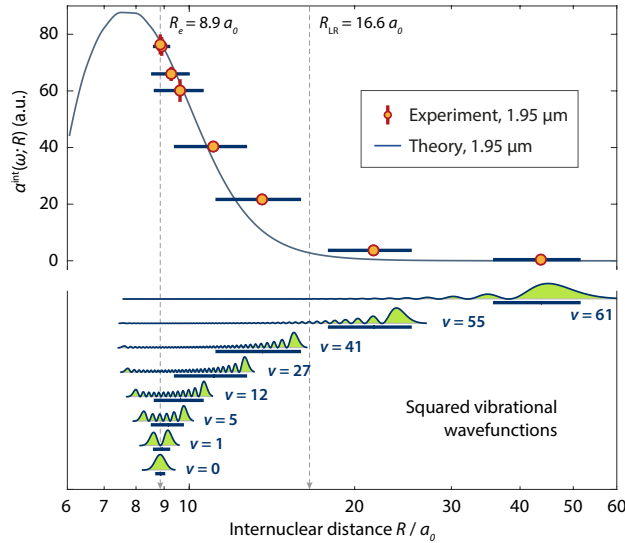


FIG. 3. Interaction-induced ac polarizability at  $\lambda = 1.95 \mu\text{m}$ . In addition to the *ab initio* result we show absolute experimental polarizabilities in relation to mean internuclear distances  $\tilde{R}$  (Table I). Horizontal bars indicate the range  $[\tilde{R}_v - S_{R_v}, \tilde{R}_v + S_{R_v}]$  of internuclear distances probed by the vibrational wavefunctions shown in the lower panel. Here  $\tilde{R}_v$  and  $S_{R_v}$  are the mean and standard deviation internuclear distances for wavefunction squared treated as a probability distribution.  $R_e$  and  $R_{\text{LR}}$  are, respectively, the equilibrium distance and the LeRoy radius [56, 57].

reduced mass  $\mu$  equals half the mass of a Sr atom. The uncertainties of the potential curve are negligible for our purposes (Supplemental Material). Figure 2 shows calculated differential dc and ac polarizabilities for  $v \leftrightarrow 62$  transitions. It should be noted that this approach is valid only when the adiabaticity condition is maintained, that is, that the ground-state potential does not cross any of the excited-state potentials if shifted upwards by the energy of the incident photon. In  $\text{Sr}_2$ , this limits the photon wavenumber to about  $8000 \text{ cm}^{-1}$  ( $1.25 \mu\text{m}$ ). Both our  $1.95\text{-}\mu\text{m}$  ( $5128\text{-cm}^{-1}$ ) laser and the room-temperature BBR spectrum are well within this margin.

We first validate the *ab initio* model using polarizabilities of the ground-state Sr atom. At dc we find a polarizability of  $+197.327$  a.u., in excellent agreement with the state-of-the-art semi-empirical value of  $+197.14(20)$  a.u. [40]. Similarly, our ac polarizability of  $+207.524$  a.u. at  $1.95 \mu\text{m}$  agrees perfectly with the value of  $+208.2(1.1)$  a.u. [54].

The key test of our model relies on a direct comparison and strong agreement of measured differential polarizability at  $1.95 \mu\text{m}$  with the calculated values (Figure 2). For example, the theoretical differential polarizability for the  $0 \leftrightarrow 62$  clock transition,  $\Delta\alpha_{0 \leftrightarrow 62}(\omega)$ , is  $-77.2$  a.u. compared to the experimental value of  $-76.4(3.6)$  a.u.. As we move to more weakly bound target states, the differential polarizabilities decrease monotonically. This can be elucidated using the  $R$ -centroid approximation [67] and the concept of a LeRoy radius  $R_{\text{LR}}$  [56, 57]. Firstly, the  $R$ -centroid approximation allows us to estimate the interaction-induced polarizability at the mean internuclear distance  $\tilde{R}_v$  of state  $v$  using the differential polarizability of a  $v \leftrightarrow 62$  transition:

$$\alpha^{\text{int}}(\omega; \tilde{R}_v) \approx -\Delta\alpha_{v \leftrightarrow 62}(\omega), \quad (3)$$

where  $\tilde{R}_v = \int_0^\infty |\Psi_v(R)|^2 R dR$ . This formula neglects the small interaction-induced polarizability of the  $v' = 62$  state. Thus, different vibrational transitions effectively serve as probes of polarizabilities, each at a different internuclear separation (Figure 3).

The range of investigated target levels from the ground  $v = 0$  state to the second-to-least bound  $v = 61$  state spans internuclear distances from  $8.86 a_0$  (approximately the equilibrium distance  $R_e$ ) to  $43.6 a_0$ . Beyond the LeRoy radius  $R_{\text{LR}} = 16.6 a_0$  the interaction-induced polarizability is negligible:  $\text{Sr}_2$  becomes a “physicist’s molecule” [48] whose polarizability is that of two strontium atoms. At shorter internuclear separations, it becomes a “chemist’s molecule” and picks up over  $80$  a.u. of extra polarizability due to molecular bonding of the two constituent atoms. The qualitative boundary between the two extremes is set by  $R_{\text{LR}} = 2(r_A + r_B)$ , where  $r_A = r_B = 4.15 a_0$  are the RMS charge radii of the two atoms [68]. By selecting vibrational levels with different mean internuclear distances, we scan the interaction-induced polarizabilities at different internuclear separations, interpolating between the two extremes of a “chemist’s” and “physicist’s” molecule.

To estimate the relative uncertainty of our theoretical model, we fit it to the experimental data by simple scaling.

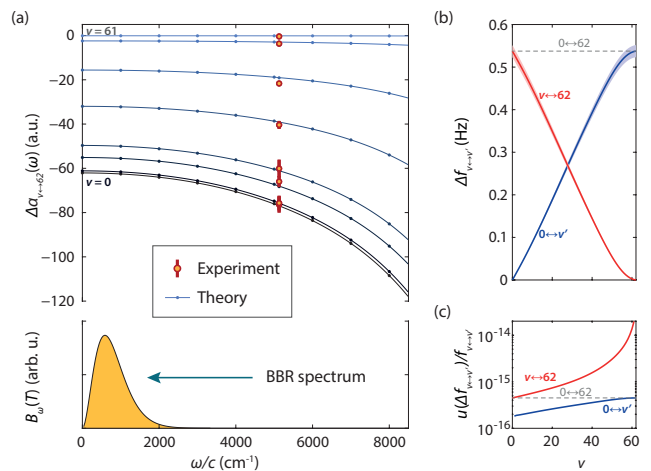


FIG. 4. (a) Differential polarizabilities for the selected clock transitions. Below, a plot of a BBR spectral radiance  $B_\omega(T)$  at 300 K. (b) Absolute BBR shift for  $0 \leftrightarrow v'$  clock transitions. (c) Relative BBR uncertainty for the same clock configurations.

The best least-squares fit is achieved by scaling the model up by  $+1.8(2.4)\%$ . This, however, is compatible with zero, showing that no model scaling is necessary; in fact, the reduced chi-square  $\chi^2/\text{dof} = 1.78$  for the scaled model ( $\text{dof} = 7$ ) is worse than  $\chi^2/\text{dof} = 1.69$  ( $\text{dof} = 8$ ) for the original, unscaled model. Thus our *ab initio* model for the molecular polarizability contains no free parameters, justifying its use for all photon wavelengths. Nevertheless, out of caution we combine the  $2.4\%$  uncertainty from the scaling factor with an additional  $1.8\%$  possible systematic error to obtain a “Type B” uncertainty [69] of  $2.6\%$ .

Finally, we calculate the BBR shift  $\Delta f_{v \leftrightarrow v'}$  by expressing it as an ac Stark shift integrated over the BBR spectrum [37, 39, 70]:

$$\Delta f_{v \leftrightarrow v'} = -\frac{1}{2h} \int_0^\infty \frac{4\pi}{\epsilon_0 c} B_\omega(T) \Delta\alpha_{v \leftrightarrow v'}(\omega) d\omega, \quad (4)$$

where the spectral radiance of the BBR field at temperature  $T$  is

$$B_\omega(T) = \frac{\hbar\omega^3}{4\pi^3 c^2} \frac{1}{\exp(\hbar\omega/k_B T) - 1}. \quad (5)$$

Typically, BBR shifts for atomic clocks are determined using a sum-over-states approach to calculate the static and dynamic terms [37, 38, 40, 70, 71], but here we already have computed the dynamic polarizabilities, so we can directly integrate the BBR shift. Since practically all of the BBR spectrum falls below any resonance frequencies in our system, we expand the polarizability in terms of Cauchy coefficients [71]:  $\Delta\alpha_{v \leftrightarrow v'}(\omega) = \Delta\alpha_{v \leftrightarrow v'}^{(0)} + \Delta\alpha_{v \leftrightarrow v'}^{(2)}\omega^2 + \Delta\alpha_{v \leftrightarrow v'}^{(4)}\omega^4 + \dots$  that we fit to tenth order to numerically calculated polarizabilities [Fig. 4(a)]. This allows us to express the BBR shift as a series:

$$\Delta f_{v \leftrightarrow v'} = \sum_{n=0,2,\dots} \Delta f_v^{(n)} = \sum_{n=0,2,\dots} -\frac{c_n \Delta\alpha_{v \leftrightarrow v'}^{(n)}}{4\pi^3 \epsilon_0 c^3} \left( \frac{k_B T}{\hbar} \right)^{4+n}, \quad (6)$$

TABLE II. Contributions to the BBR shift at 300 K for the  $0 \leftrightarrow 1$  and  $0 \leftrightarrow 62$  transitions.

$n$	$c_n$	$\Delta f_{0 \leftrightarrow 1}^{(n)}$ (Hz)	$\Delta f_{0 \leftrightarrow 1}^{(n)}/f_{0 \leftrightarrow 1}$	$\Delta f_{0 \leftrightarrow 62}^{(n)}$ (Hz)	$\Delta f_{0 \leftrightarrow 62}^{(n)}/f_{0 \leftrightarrow 62}$
0	$\pi^4/15$	+0.0081	$+6.8 \times 10^{-15}$	+0.53	$+1.7 \times 10^{-14}$
2	$8\pi^6/63$	$+6.1 \times 10^{-5}$	$+5.1 \times 10^{-17}$	+0.0033	$+1.0 \times 10^{-16}$
4	$8\pi^8/15$	$+6.5 \times 10^{-7}$	$+5.5 \times 10^{-19}$	$+6.3 \times 10^{-5}$	$+2.0 \times 10^{-18}$
$\eta$ (%)		0.54		0.62	

where the Planck integrals  $c_n = \int_0^\infty u^{3+n}/(e^u - 1)du$  are given in Table II (Supplemental Material). The leading term is the well known static contribution to the BBR shift [39, 40], while further terms constitute a dynamic correction  $\eta$  on the order of 0.5–0.6 % (Table II). Here terms beyond the second order are negligible.

Since the molecular clock uniquely provides an array of available clock states, we calculate the BBR shift for other clock transitions. In Fig. 4(b), we plot the BBR shift for  $v \leftrightarrow 62$  transitions,  $\Delta f_{v \leftrightarrow 62}$  (red line). For our previously measured clock transition [41]  $\Delta f_{0 \leftrightarrow 62} = +538(15)$  mHz, which leads to a BBR contribution to fractional uncertainty of  $u(\Delta f_{v \leftrightarrow v'})/f_{v \leftrightarrow v'} = 4.7 \times 10^{-16}$ . We further find that the BBR contribution to fractional uncertainty of the molecular clock transition can be reduced by strategically selecting  $0 \leftrightarrow v'$  clock transitions (blue line) between deeply bound vibrational states [Fig. 4(c)]. This configuration could allow fractional uncertainties as low as  $1.8 \times 10^{-16}$ , a factor of  $\sim 2.5$  lower than the  $0 \leftrightarrow 62$  transition.

Additionally, clock transitions between deeply bound states could allow for magic wavelengths that are further detuned from excited molecular resonances as there would be a smaller polarizability gap to overcome. That in turn could improve molecular trap lifetimes and Q-factors. The latter can also be improved by switching to a vertical lattice geometry. On the flipside, this requires the use of STIRAP [43, 72, 73] to initialize the molecule population in a deeply-bound state, increasing experimental complexity. An experimental setup combining these ideas is now being constructed.

In the future, our technique can be pushed further. The polarizability measurement relies on frequency shifts that could be determined at the full Hz-level clock accuracy. It also depends on semiempirical atomic polarizabilities that currently contribute about 10% of the error bar. Eventually, however, with better measurements the *ab initio* model will cease to agree with experiment. In such a case scaling is an option, but an entirely different approach could be also taken where polarizabilities are measured at several different wavelengths and Cauchy coefficients are fitted directly to experiment.

In conclusion, we have determined the BBR shift in a strontium molecular lattice clock. We do so by leveraging agreement between precision spectroscopy and modern quantum chemistry to provide a robust description of the polarizability behavior of ground state  $\text{Sr}_2$  molecules. Specifically, we performed ac Stark shift spectroscopy of several molecular clock

transitions throughout the ground state potential induced by an additional 1.95- $\mu\text{m}$  laser. These measurements were in excellent agreement with *ab initio* calculations of molecular polarizability, lending credence to extending this model to other wavelengths from dc to 1.25  $\mu\text{m}$ . This determination will allow us to control the BBR shift systematic to the  $10^{-16}$  level. By selecting a clock transition between deeply bound vibrational states ( $v < 10$ ), we could further suppress the BBR effect. In the future, additional measurements of ac or dc Stark shifts, such as by direct application of a dc electric field [37] or ac Stark measurement with a  $\text{CO}_2$  laser [74, 75], could further constrain the theoretical model resulting in improved control of the BBR systematic. A next-generation molecular clock could search for new interactions beyond the Standard Model or probe the variations of fundamental constants. This work paves the way towards mHz-level spectroscopy in  $\text{Sr}_2$  molecules.

We thank M. Safronova for providing theoretical atomic polarizabilities, P. S. Żuchowski for fruitful discussions, I. Majewska for involvement and discussions at the early stages of this project and J. Dai, D. Mitra and Q. Sun for experimental assistance. This work was supported by NSF grant PHY-1911959, AFOSR MURI FA9550-21-1-0069, ONR grant N00014-21-1-2644, the Brown Science Foundation, and the Polish National Science Centre (NCN) grant 2016/21/B/ST4/03877. M. B. was partially funded by the Polish National Agency for Academic Exchange within the Bekker Programme, project PPN/BEK/2020/1/00306/U/00001, and by NCN, grant 2017/25/B/ST4/01486. W.S. acknowledges Polish high-performance computing infrastructure PLGrid (HPC Centers: ACK Cyfronet AGH) for providing computer facilities and support within computational grant no. PLG/2022/015675.

\* These authors contributed equally to this work.

† mateusz@cold-molecules.com

‡ tanya.zelevinsky@columbia.edu

- [1] M. Takamoto, F.-L. Hong, R. Higashi, and H. Katori, An optical lattice clock, *Nature* **435**, 321 (2005).
- [2] H. Katori, Optical lattice clocks and quantum metrology, *Nature Photonics* **5**, 203 (2011).
- [3] W. F. McGrew, X. Zhang, R. J. Fasano, S. A. Schäffer, K. Beloy, D. Nicolodi, R. C. Brown, N. Hinkley, G. Milani, M. Schioppo, T. H. Yoon, and A. D. Ludlow, Atomic clock performance enabling geodesy below the centimetre level, *Nature* **564**, 87 (2018).
- [4] T. Bothwell, D. Kedar, E. Oelker, J. M. Robinson, S. L. Bromley, W. L. Tew, J. Ye, and C. J. Kennedy, JILA SrI optical lattice clock with uncertainty of  $2 \times 10^{-18}$ , *Metrologia* **56**, 065004 (2019).
- [5] W. F. McGrew, X. Zhang, H. Leopardi, R. J. Fasano, D. Nicolodi, K. Beloy, J. Yao, J. A. Sherman, S. A. Schäffer, J. Savory, R. C. Brown, S. Römisich, C. W. Oates, T. E. Parker, T. M. Fortier, and A. D. Ludlow, Towards the optical second: verifying optical clocks at the SI limit, *Optica* **6**, 448 (2019).
- [6] J. Lodewyck, On a definition of the si second with a set of opti-

cal clock transitions, *Metrologia* **56**, 055009 (2019).

[7] S. Bize, The unit of time: Present and future directions, *Comptes Rendus Physique* **20**, 153 (2019).

[8] M. Borkowski, Optical Lattice Clocks with Weakly Bound Molecules, *Physical Review Letters* **120**, 083202 (2018).

[9] S. S. Kondov, C.-H. Lee, K. H. Leung, C. Liedl, I. Majewska, R. Moszynski, and T. Zelevinsky, Molecular lattice clock with long vibrational coherence, *Nature Physics* **15**, 1118 (2019).

[10] J. Kobayashi, A. Ogino, and S. Inouye, Measurement of the variation of electron-to-proton mass ratio using ultracold molecules produced from laser-cooled atoms, *Nature Communications* **10**, 3771 (2019).

[11] D. Hanneke, B. Kuzhan, and A. Lunstad, Optical clocks based on molecular vibrations as probes of variation of the proton-to-electron mass ratio, *Quantum Science and Technology* **6**, 014005 (2020).

[12] G. Barontini, L. Blackburn, V. Boyer, F. Butuc-Mayer, X. Calmet, J. R. Crespo López-Urrutia, E. A. Curtis, B. Darquié, J. Dunningham, N. J. Fitch, E. M. Forgan, K. Georgiou, P. Gill, R. M. Godun, J. Goldwin, *et al.*, Measuring the stability of fundamental constants with a network of clocks, *EPJ Quantum Technology* **9**, 12 (2022).

[13] E. J. Salumbides, W. Ubachs, and V. I. Korobov, Bounds on fifth forces at the sub-Å length scale, *Journal of Molecular Spectroscopy* **300**, 65 (2014).

[14] J. Biesheuvel, J.-P. Karr, L. Hilico, K. Eikema, W. Ubachs, and J. Koelemeij, Probing QED and fundamental constants through laser spectroscopy of vibrational transitions in HD<sup>+</sup>, *Nature Communications* **7**, 10385 (2016).

[15] M. Borkowski, A. A. Buchachenko, R. Ciuryło, P. S. Julienne, H. Yamada, Y. Kikuchi, Y. Takasu, and Y. Takahashi, Weakly bound molecules as sensors of new gravitylike forces, *Scientific Reports* **9**, 14807 (2019).

[16] B. Heacock, T. Fujii, R. W. Haun, A. Henins, K. Hirota, T. Hosobata, M. G. Huber, M. Kitaguchi, D. A. Pushin, H. Shimizu, M. Takeda, R. Valdillez, Y. Yamagata, and A. R. Young, Pendellösung interferometry probes the neutron charge radius, lattice dynamics, and fifth forces, *Science* **373**, 1239 (2021).

[17] S. Schiller and V. Korobov, Tests of time independence of the electron and nuclear masses with ultracold molecules, *Phys. Rev. A* **71**, 032505 (2005).

[18] D. DeMille, S. Sainis, J. Sage, T. Bergeman, S. Kotochigova, and E. Tiesinga, Enhanced sensitivity to variation of me/mp in molecular spectra, *Physical Review Letters* **100**, 043202 (2008).

[19] K. Beloy, A. W. Hauser, A. Borschevsky, V. V. Flambaum, and P. Schwerdtfeger, Effect of Alpha variation on the vibrational spectrum of Sr<sub>2</sub>, *Phys. Rev. A* **84**, 062114 (2011).

[20] S. Schiller, D. Bakalov, and V. I. Korobov, Simplest molecules as candidates for precise optical clocks, *Phys. Rev. Lett.* **113**, 023004 (2014).

[21] M. Kajita, G. Gopakumar, M. Abe, M. Hada, and M. Keller, Test of  $m_p/m_e$  changes using vibrational transitions in n<sub>2</sub><sup>+</sup>, *Phys. Rev. A* **89**, 032509 (2014).

[22] M. Germann, X. Tong, and S. Willitsch, Observation of electric-dipole-forbidden infrared transitions in cold molecular ions, *Nature Physics* **10**, 820 (2014).

[23] P. Wcisło, P. Ablewski, K. Beloy, S. Bilicki, M. Bober, R. Brown, R. Fasano, R. Ciuryło, H. Hachisu, T. Ido, J. Lodewyck, A. Ludlow, W. McGrew, P. Morzyński, D. Niccolodi, M. Schioppo, M. Sekido, R. Le Targat, P. Wolf, X. Zhang, B. Zjawin, and M. Zawada, New bounds on dark matter coupling from a global network of optical atomic clocks, *Science Advances* **4**, eaau4869 (2018).

[24] M. S. Safronova, The search for variation of fundamental constants with clocks, *Annalen der Physik* **531**, 1800364 (2019).

[25] N. R. Hutzler, Polyatomic molecules as quantum sensors for fundamental physics, *Quantum Science and Technology* **5**, 044011 (2020).

[26] R. Lange, N. Huntemann, J. M. Rahm, C. Sanner, H. Shao, B. Lipphardt, C. Tamm, S. Weyers, and E. Peik, Improved limits for violations of local position invariance from atomic clock comparisons, *Phys. Rev. Lett.* **126**, 011102 (2021).

[27] R. Le Targat, L. Lorini, Y. Le Coq, M. Zawada, J. Guéna, M. Abgrall, M. Gurov, P. Rosenbusch, D. G. Rovera, B. Nagórny, R. Gartman, P. G. Westergaard, M. E. Tobar, M. Lours, G. Santarelli, A. Clairon, S. Bize, P. Laurent, P. Lemonde, and J. Lodewyck, Experimental realization of an optical second with strontium lattice clocks, *Nature Communications* **4**, 2109 (2013).

[28] S. Falke, N. Lemke, C. Grebing, B. Lipphardt, S. Weyers, V. Gerginov, N. Huntemann, C. Hagemann, A. Al-Masoudi, S. Häfner, S. Vogt, U. Sterr, and C. Lisdat, A strontium lattice clock with  $3 \times 10^{-17}$  inaccuracy and its frequency, *New Journal of Physics* **16**, 073023 (2014).

[29] T. Nicholson, S. Campbell, R. Hutson, G. Marti, B. Bloom, R. McNally, W. Zhang, M. Barrett, M. Safronova, G. Strouse, W. Tew, and J. Ye, Systematic evaluation of an atomic clock at  $2 \times 10^{-18}$  total uncertainty, *Nature Communications* **6**, 6896 (2015).

[30] S. B. Koller, J. Grotti, S. Vogt, A. Al-Masoudi, S. Dörscher, S. Häfner, U. Sterr, and C. Lisdat, Transportable optical lattice clock with  $7 \times 10^{-17}$  uncertainty, *Phys. Rev. Lett.* **118**, 073601 (2017).

[31] Y. Hisai, D. Akamatsu, T. Kobayashi, K. Hosaka, H. Inaba, F.-L. Hong, and M. Yasuda, Improved frequency ratio measurement with <sup>87</sup>Sr and <sup>171</sup>Yb optical lattice clocks at NMIJ, *Metrologia* **58**, 015008 (2021).

[32] N. Ohmae, M. Takamoto, Y. Takahashi, M. Kokubun, K. Araki, A. Hinton, I. Ushijima, T. Muramatsu, T. Furumiya, Y. Sakai, N. Moriya, N. Kamiya, K. Fujii, R. Muramatsu, T. Shiimado, and H. Katori, Transportable Strontium Optical Lattice Clocks Operated Outside Laboratory at the Level of  $10^{-18}$  Uncertainty, *Advanced Quantum Technologies* **4**, 2100015 (2021).

[33] I. Ushijima, M. Takamoto, M. Das, T. Ohkubo, and H. Katori, Cryogenic optical lattice clocks, *Nature Photonics* **9**, 185 (2015).

[34] P. Ablewski, M. Bober, and M. Zawada, Emissivities of vacuum compatible materials: towards minimising blackbody radiation shift uncertainty in optical atomic clocks at room temperatures, *Metrologia* **57**, 035004 (2020).

[35] V. I. Yudin, A. V. Taichenachev, M. Y. Basalaev, O. N. Prudnikov, H. A. Fürst, T. E. Mehlstäubler, and S. N. Bagayev, Combined atomic clock with blackbody-radiation-shift-induced instability below  $10^{-19}$  under natural environment conditions, *New Journal of Physics* **23**, 023032 (2021).

[36] T. Middelmann, C. Lisdat, S. Falke, J. S. R. Vellore Winfred, F. Riehle, and U. Sterr, Tackling the blackbody shift in a strontium optical lattice clock, *IEEE Transactions on Instrumentation and Measurement* **60**, 2550 (2011).

[37] T. Middelmann, S. Falke, C. Lisdat, and U. Sterr, High accuracy correction of blackbody radiation shift in an optical lattice clock, *Phys. Rev. Lett.* **109**, 263004 (2012).

[38] C. Lisdat, S. Dörscher, I. Nosske, and U. Sterr, Blackbody radiation shift in strontium lattice clocks revisited, *Phys. Rev. Res.* **3**, L042036 (2021).

[39] S. G. Porsev and A. Derevianko, Multipolar theory of blackbody radiation shift of atomic energy levels and its implications

for optical lattice clocks, *Phys. Rev. A* **74**, 020502 (2006).

[40] M. S. Safranova, S. G. Porsev, U. I. Safranova, M. G. Kozlov, and C. W. Clark, Blackbody-radiation shift in the Sr optical atomic clock, *Physical Review A* **87**, 012509 (2013).

[41] K. H. Leung, B. Iritani, E. Tiberi, I. Majewska, M. Borkowski, R. Moszynski, and T. Zelevinsky, Terahertz vibrational molecular clock with systematic uncertainty at the  $10^{-14}$  level, *Phys. Rev. X* **13**, 011047 (2023).

[42] K. H. Leung, I. Majewska, H. Bekker, C.-H. Lee, E. Tiberi, S. S. Kondov, R. Moszynski, and T. Zelevinsky, Transition strength measurements to guide magic wavelength selection in optically trapped molecules, *Phys. Rev. Lett.* **125**, 153001 (2020).

[43] K. H. Leung, E. Tiberi, B. Iritani, I. Majewska, R. Moszynski, and T. Zelevinsky, Ultracold  $^{88}\text{Sr}_2$  molecules in the absolute ground state, *New Journal of Physics* **23**, 115002 (2021).

[44] T. Zelevinsky, M. M. Boyd, A. D. Ludlow, T. Ido, J. Ye, R. Ciuryło, P. Naidon, and P. S. Julienne, Narrow Line Photoassociation in an Optical Lattice, *Physical Review Letters* **96**, 203201 (2006).

[45] B. H. McGuyer, M. McDonald, G. Z. Iwata, M. G. Tarallo, A. T. Grier, F. Apfelbeck, and T. Zelevinsky, High-precision spectroscopy of ultracold molecules in an optical lattice, *New J. Phys* **17**, 055004 (2015).

[46] S. H. Autler and C. H. Townes, Stark effect in rapidly varying fields, *Phys. Rev.* **100**, 703 (1955).

[47] C. H. Townes and A. L. Schawlow, *Microwave spectroscopy* (Dover Publications, 1975).

[48] K. M. Jones, E. Tiesinga, P. D. Lett, and P. S. Julienne, Ultracold photoassociation spectroscopy: Long-range molecules and atomic scattering, *Reviews of Modern Physics* **78**, 483 (2006).

[49] Y. N. Martinez de Escobar, P. G. Mickelson, P. Pellegrini, S. B. Nagel, A. Traverso, M. Yan, R. Côté, and T. C. Killian, Two-photon photoassociative spectroscopy of ultracold  $^{88}\text{Sr}$ , *Phys. Rev. A* **78**, 062708 (2008).

[50] M. Kitagawa, K. Enomoto, K. Kasa, Y. Takahashi, R. Ciuryło, P. Naidon, and P. S. Julienne, Two-color photoassociation spectroscopy of ytterbium atoms and the precise determinations of s-wave scattering lengths, *Physical Review A* **77**, 012719 (2008).

[51] E. Tiesinga, P. J. Mohr, D. B. Newell, and B. N. Taylor, Codata recommended values of the fundamental physical constants: 2018, *Rev. Mod. Phys.* **93**, 025010 (2021).

[52] R. V. Pound, Electronic frequency stabilization of microwave oscillators, *Review of Scientific Instruments* **17**, 490 (1946).

[53] R. W. Drever, J. L. Hall, F. V. Kowalski, J. Hough, G. Ford, A. Munley, and H. Ward, Laser phase and frequency stabilization using an optical resonator, *Applied Physics B* **31**, 97 (1983).

[54] M. S. Safranova, private communication (2023).

[55] M. McDonald, B. H. McGuyer, G. Z. Iwata, and T. Zelevinsky, Thermometry via light shifts in optical lattices, *Phys. Rev. Lett.* **114**, 023001 (2015).

[56] R. J. Le Roy and R. B. Bernstein, Dissociation Energy and Long-Range Potential of Diatomic Molecules from Vibrational Spacings of Higher Levels, *The Journal of Chemical Physics* **52**, 3869 (1970).

[57] R. J. Le Roy, *Molecular Spectroscopy - Volume I, A Specialist Periodical Report of the Chemical Society* (The Chemical Society, London, 1973) pp. 113–171.

[58] K. D. Nanda and A. I. Krylov, Static polarizabilities for excited states within the spin-conserving and spin-flipping equation-of-motion coupled-cluster singles and doubles formalism: Theory, implementation, and benchmarks, *The Journal of Chemical Physics* **145**, 204116 (2016).

[59] E. Epifanovsky, A. T. B. Gilbert, X. Feng, J. Lee, Y. Mao, N. Mardirossian, P. Pokhilko, A. F. White, M. P. Coons, A. L. Dempwolff, Z. Gan, D. Hait, P. R. Horn, L. D. Jacobson, I. Kaliman, *et al.*, Software for the frontiers of quantum chemistry: An overview of developments in the Q-Chem 5 package, *The Journal of Chemical Physics* **155**, 084801 (2021).

[60] I. S. Lim, H. Stoll, and P. Schwerdtfeger, Relativistic small-core energy-consistent pseudopotentials for the alkaline-earth elements from Ca to Ra, *The Journal of Chemical Physics* **124**, 034107 (2006).

[61] A. Dalgarno, A. L. Ford, and J. C. Browne, Direct Sum-of-States Calculations of the Frequency-Dependent Polarizability of  $\text{H}_2$ , *Physical Review Letters* **27**, 1033 (1971).

[62] J. M. Brown and A. Carrington, *Rotational Spectroscopy of Diatomic Molecules* (Cambridge University Press, Cambridge, 2003).

[63] T. G. A. Heijmen, R. Moszynski, P. E. S. Wormer, and A. van der Avoird, Symmetry-adapted perturbation theory applied to interaction-induced properties of collisional complexes, *Molecular Physics* **89**, 81 (1996).

[64] D. T. Colbert and W. H. Miller, A novel discrete variable representation for quantum mechanical reactive scattering via the S-matrix Kohn method, *J. Chem. Phys.* **96**, 1982 (1992).

[65] E. Tiesinga, C. J. Williams, and P. S. Julienne, Photoassociative spectroscopy of highly excited vibrational levels of alkali-metal dimers: Green-function approach for eigenvalue solvers, *Phys. Rev. A* **57**, 4257 (1998).

[66] A. Stein, H. Knöckel, and E. Tiemann,  $^1\text{S}+^1\text{S}$  asymptote of  $\text{Sr}_2$  studied by Fourier-transform spectroscopy, *Eur. Phys. J. D* **57**, 171 (2010).

[67] P. A. Fraser, A method of determining the electronic transition moment for diatomic molecules, *Canadian Journal of Physics* **32**, 515 (1954).

[68] E. Clementi, D. L. Raimondi, and W. P. Reinhardt, Atomic Screening Constants from SCF Functions. II. Atoms with 37 to 86 Electrons, *J. Chem. Phys.* **47**, 1300 (1967).

[69] B. N. Taylor and C. E. Kuyatt, *NIST Technical Note 1297. Guidelines for evaluating and expressing the uncertainty of NIST measurement results* (US Department of Commerce, Technology Administration, National Institute of Standards and Technology, 1994).

[70] J. W. Farley and W. H. Wing, Accurate calculation of dynamic Stark shifts and depopulation rates of Rydberg energy levels induced by blackbody radiation. Hydrogen, helium, and alkali-metal atoms, *Phys. Rev. A* **23**, 2397 (1981).

[71] J. Mitroy, M. S. Safranova, and C. W. Clark, Theory and applications of atomic and ionic polarizabilities, *Journal of Physics B: Atomic, Molecular and Optical Physics* **43**, 202001 (2010).

[72] K. Bergmann, H. Theuer, and B. W. Shore, Coherent population transfer among quantum states of atoms and molecules, *Reviews of Modern Physics* **70**, 1003 (1998).

[73] N. V. Vitanov, A. A. Rangelov, B. W. Shore, and K. Bergmann, Stimulated Raman adiabatic passage in physics, chemistry, and beyond, *Reviews of Modern Physics* **89**, 1 (2017).

[74] J. Chen, To simulate blackbody radiation frequency shift in cesium fountain frequency standard with  $\text{CO}_2$  laser, *IEEE Transactions on Ultrasonics, Ferroelectrics and Frequency Control* **53**, 1685 (2006).

[75] K. J. Arnold, R. Kaewuam, A. Roy, T. R. Tan, and M. D. Barrett, Blackbody radiation shift assessment for a lutetium ion clock, *Nature Communications* **9**, 1650 (2018).

# Supplemental Material: Accurate Determination of Blackbody Radiation Shifts in a Strontium Molecular Lattice Clock

B. Iritani<sup>1,\*</sup> E. Tiberi<sup>1,\*</sup> W. Skomorowski<sup>2</sup> R. Moszynski<sup>3</sup> M. Borkowski<sup>1,4,5,†</sup> and T. Zelevinsky<sup>1,‡</sup>

<sup>1</sup>Department of Physics, Columbia University, 538 West 120th Street, New York, NY 10027-5255, USA

<sup>2</sup>Centre of New Technologies, University of Warsaw, Banacha 2c, 02-097 Warsaw, Poland

<sup>3</sup>Quantum Chemistry Laboratory, Department of Chemistry,  
University of Warsaw, Pasteura 1, 02-093 Warsaw, Poland

<sup>4</sup>Van der Waals-Zeeman Institute, Institute of Physics, University of Amsterdam,  
Science Park 904, 1098 XH Amsterdam, The Netherlands

<sup>5</sup>Institute of Physics, Faculty of Physics, Astronomy and Informatics,  
Nicolaus Copernicus University, Grudziadzka 5, 87-100 Toruń, Poland

## S1. DETERMINATION OF MAGIC WAVELENGTHS

For each of the investigated molecular clock transitions we have determined its corresponding magic wavelength. Our process for finding magic wavelengths consists of several steps and combines theoretical modelling and experiment.

The polarizability of the initial weakly-bound molecular state is approximately twice the polarizability of the constituent strontium atoms and only has a very weak dependence on the wavelength of the lattice laser. On the other hand, the polarizability for the deeply-bound states has many resonances due to strong transitions to the vibrational states supported by the  $1_u$  state correlating to the  $^1\text{S}_0 + ^3\text{P}_1$  asymptote. We exploit this to tune the polarizability of the deeply-bound state to that of the weakly-bound state to achieve the magic condition.

We first employ a theoretical interaction model to calculate transition dipole moments for transitions from the deeply

bound molecular clock state  $v$  to vibrational states in the  $(1) 1_u$  excited-state potential. We select  $(1) 1_u$  states such that the line strength  $S$  is greater than  $\sim 10^{-5} e^2 a_0^2$  (here  $e$  is the electron charge,  $a_0$  is the Bohr radius) [S1]. Then, we predict the magic wavelengths by calculating the differential polarizability of the clock transition using a sum-over-states approach. This provides a starting point for the final experimental search. By varying the power of the lattice beam, we measure the Stark shift  $\Delta_{\text{Stark}}$  of the molecular clock line at several wavelengths spread over  $\sim 10$  GHz centered around the predicted magic wavelength (Figure S1). Then, we fit a simple formula

$$\Delta_{\text{Stark}}(\lambda) = \frac{a}{\lambda - \lambda_0} + b \quad (\text{S1})$$

to lattice Stark shifts measured as a function of frequency to find the zero crossing,  $\lambda_{\text{magic}} = \lambda_0 - a/b$ . Our lattice wavelength is stabilized to a wavemeter at  $\sim 30$  MHz precision. It should also be pointed out that the absolute calibration of the wavemeter is on the order of 0.001 nm as indicated in Table 1 in the main text.

## S2. MEASUREMENTS OF LINE POSITIONS

We measure the relative binding energies by scanning the frequency difference between the two Raman lasers, detuned by  $\sim 30$  MHz from the intermediate state, a molecular level of  $(1) 0_u^+$  symmetry. The Raman pump laser is locked to a high finesse cavity, and the repetition rate of an optical frequency comb is in turn referenced to this laser. The carrier envelope offset of the frequency comb, as well as acousto-optical modulators used on both Raman lasers, are referenced to a commercial rubidium clock at a  $\sim 10^{-12}$  precision [S2]. Finally, the anti-Stokes laser of the Raman pair is phase-locked to the optical frequency comb.

The line positions are measured through scans of the relative Raman frequency (Figure S2). We fit the scans with a Lorentzian lineshape with a background,

$$n(\Delta) = n_0 - \frac{A}{2\pi} \frac{\gamma}{(\Delta - \Delta_c)^2 + (\gamma/2)^2}, \quad (\text{S2})$$

where  $n_0$  is the background dissociated atom number,  $A$  is the area,  $\gamma$  is the full width at half maximum, and  $\Delta_c$  is the center

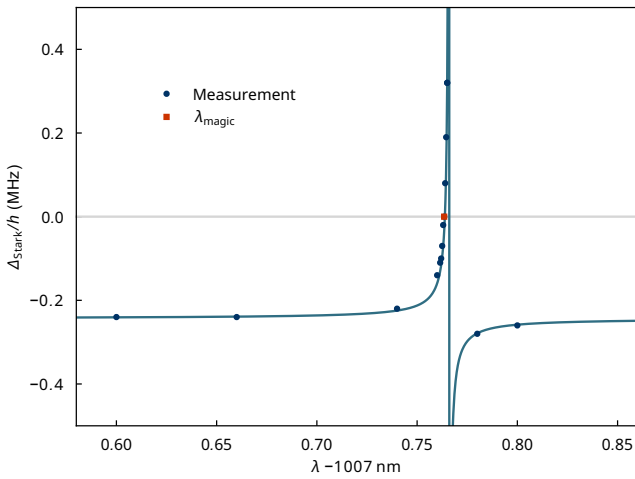


FIG. S1. Search for the magic wavelength on the example of the  $v = 12 \leftrightarrow v' = 62$  molecular clock transition. Points denote the experimental lattice-induced ac Stark shift as a function of lattice laser wavelength  $\lambda$ . The fitted function is Eq. (S1). The red square indicates the magic wavelength  $\lambda_{\text{magic}} = 1007.7634(10)$  nm, where the Stark shift  $\Delta_{\text{Stark}}$  is cancelled out.

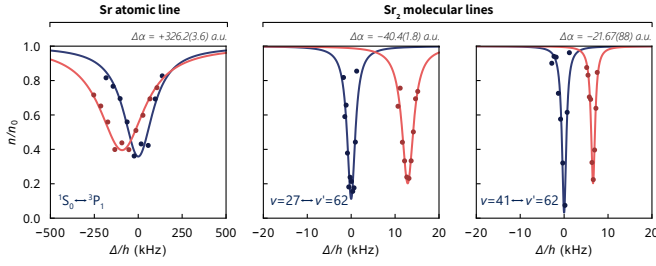


FIG. S2. Example lineshapes seen in our ac Stark shift measurements. To determine the differential ac polarizability, we measure a lineshape each with the extra ac Stark laser off (dark blue) and on (light red). To determine the differential polarizabilities  $\Delta\alpha$  we measure ratios of ac Stark shift slopes between different transitions. As an absolute reference we used the narrow  $^1S_0 \leftrightarrow ^3P_1$  atomic intercombination transition with a known  $\Delta\alpha = +326.2(3.6)$  a.u. [S3]. The molecular ac Stark shifts would be compared to a common  $27 \leftrightarrow 62$  transition which would then be calibrated to the atomic line.

frequency. We typically operate with 1 kHz peak widths and can measure peak position to  $\sim 100$  Hz.

Since precise determination of transition frequencies is not the main purpose of this paper, we did not characterize the Stark shifts experimentally. Instead, we calculate a conservative upper bound on the uncertainty of the binding energy by combining estimated lattice and Raman laser Stark shifts.

Using the Stark shift measured during magic wavelength determination, we fit a linear slope to Stark shift vs. lattice frequency near the operational magic wavelength. We then use this slope to convert the wavemeter-limited uncertainty of the lattice wavelength to a Stark shift, and take this Stark shift as our lattice contribution to the uncertainty of the binding energy.

Using measured laser power and waist, as well as *ab initio* polarizabilities calculated using the sum-over-states approach [S4], we calculate the Raman Stark shifts,

$$\Delta f_{\text{clock}} = \frac{I_R}{2h\epsilon_0 c} [\alpha_0(\lambda_R) - \alpha_{62}(\lambda_R)], \quad (\text{S3})$$

where  $I_R$  is the intensity of each Raman laser,  $\alpha$  is polarizability for each vibrational state, and  $\lambda$  is the wavelength. We note that contributions from the Raman lasers have opposite signs [S5]. We assign an additional conservative value of 50% to the *ab initio* polarizabilities, significantly larger than the discrepancy observed in comparison with measured polarizability ratios [S2].

After estimating the lattice and Raman Stark shifts individually, we combine them to get total uncertainty on binding energy position. We find that the lattice Stark shift is about an order of magnitude greater than Raman Stark shift.

### S3. FINITE SAMPLE TEMPERATURE

Our experiment relies on Stark-induced shifts to molecular clock lines. Here we estimate the effect of finite sample tem-

perature on the determination of differential polarizabilities from observed shifts.

In the absence of the Stark laser the molecules, whether in their initial ( $v$ ), or target ( $v'$ ) vibrational states are trapped in the same magic-wavelength lattice potential. For a single lattice site this may be approximated by a harmonic trap potential:

$$V(x, y, z) = \frac{1}{2} M \omega_r^2 (x^2 + y^2) + \frac{1}{2} M \omega_z^2 z^2. \quad (\text{S4})$$

Here  $M$  is the mass of the molecule and  $\omega_{r,z}$  are the radial ( $r$ ) and axial ( $z$ ) trapping frequencies.

We induce an ac Stark shift on the molecular clock  $v \leftrightarrow v'$  transition by adding an extra collimated laser coaligned with the lattice which gives rise to an extra potential,

$$W(x, y, z) = \frac{1}{2} M \Omega_{v,v'}^2 (x^2 + y^2) - U_{v,v'}, \quad (\text{S5})$$

where  $\Omega_{v,v'}$  are the state-dependent radial trapping frequencies and  $U_{v,v'}$  are the extra trapping depths. Both  $\Omega_{v,v'}^2$  and  $U_{v,v'}$  are directly proportional to the ac polarizabilities  $\alpha_{v,v'}$  that we aim to measure. The increase in trap depth  $U_{v,v'}$  leads to a temperature-independent line shift that is the basis for our experiment. However, the extra trapping frequency leads to a non-trivial temperature-dependent shift that we will evaluate here.

The total trapping potential of the combined laser beams is

$$V_{v,v'} + W_{v,v'} = \frac{1}{2} M (\omega_r^2 + \Omega_{v,v'}^2) (x^2 + y^2) + \frac{1}{2} M \omega_z^2 z^2 - U_{v,v'}. \quad (\text{S6})$$

This is equivalent to a three-dimensional harmonic oscillator with state-dependent trapping frequencies. As carrier transitions preserve the motional quantum numbers, the total shift may be evaluated as a difference of the quantum thermal averages of the trapping hamiltonians  $H_{v,v'} = T + V + W_{v,v'}$ :

$$\begin{aligned} \langle \delta E \rangle &= \langle H_{v'} \rangle - \langle H_v \rangle \\ &= -\Delta U + \hbar \Delta \omega [\langle n_x \rangle + \langle n_y \rangle + 1], \end{aligned} \quad (\text{S7})$$

where  $\Delta U = U_{v'} - U_v$  and the change in radial trapping frequency is

$$\Delta \omega = \sqrt{\omega_r^2 + \Omega_{v'}^2} - \sqrt{\omega_r^2 + \Omega_{v'}^2 - \Delta(\Omega_{v,v'}^2)}. \quad (\text{S8})$$

For us the transition-dependent term  $\Delta(\Omega_{v,v'}^2) = \Omega_{v'}^2 - \Omega_v^2$  is on the whole substantially smaller than either of the trapping frequencies  $\Omega_v^2$  or  $\omega_r^2$ , hence we can expand  $\Delta \omega$  as

$$\Delta \omega \approx \sqrt{\omega_r^2 + \Omega_{v'}^2} \left( \frac{1}{2} \frac{\Delta(\Omega^2)}{\omega_r^2 + \Omega_{v'}^2} - \frac{1}{8} \left( \frac{\Delta(\Omega^2)}{\omega_r^2 + \Omega_{v'}^2} \right)^2 \right). \quad (\text{S9})$$

Importantly, the first term is linear in the measured differential polarizability as  $\Delta(\Omega_{v,v'}^2)$  is directly proportional to  $\Delta\alpha_{v,v'}$ .

The mean vibrational quantum numbers for radial motion can be evaluated by averaging over the grand canonical ensemble:

$$\langle n_{x,y} \rangle = \frac{1}{Z} \sum_{n=1}^{\infty} e^{\frac{-E_n(x,y)}{k_B T}} \approx \frac{k_B T}{\hbar \omega_r}, \quad (\text{S10})$$

$$(\text{S11})$$

where we used the partition function [S6]

$$Z = \text{Tr}(e^{-H_v/k_B T}) = \frac{1}{2} \text{csch}(\hbar \omega / 2k_B T). \quad (\text{S12})$$

Finally, the total thermally averaged shift to the line is

$$\langle \delta E \rangle = -\Delta U + k_B T \frac{\Delta \omega}{\omega_r}. \quad (\text{S13})$$

The first term is the temperature-independent ac Stark shift. The second term is a temperature-dependent correction.

In our experiment the incoming lattice beam has a power of  $P_l = 0.27 \text{ W}$  and a waist of  $w_l = 36 \mu\text{m}$ . For all the measured transitions the wavelength of the lattice is chosen to achieve a magic condition. This means that the polarizability at the lattice wavelength for both the initial  $v'$  and target  $v$  molecular states is the same and can be modeled as twice the atomic polarizability. For the magic wavelengths ranging from  $\lambda_{\text{magic}} = 996.4379 \text{ nm}$  to  $\lambda_{\text{magic}} = 1016.9714 \text{ nm}$  the atomic polarizabilities range from  $\alpha_{\text{magic}} = 250.2 \text{ a.u.}$  to  $\alpha_{\text{magic}} = 247.6 \text{ a.u.}$ , respectively. This corresponds to total atomic trap depths

$$U_l = 4\alpha P_l / (\pi w_l^2 c \epsilon_0) \quad (\text{S14})$$

between  $622 \text{ kHz} \times h$  and  $616 \text{ kHz} \times h$  (approximately  $30 \mu\text{K}$ ). The factor of four stems from constructive interference between the incident and reflected lattice beams. Conversely, the radial trapping frequencies

$$\omega_r = \frac{2}{w_l} \sqrt{U_l/M} \quad (\text{S15})$$

of  $\omega_r = 2\pi \times 469.9 \text{ Hz}$  to  $2\pi \times 467.5 \text{ Hz}$ . The molecular sample temperature is estimated at  $5 \mu\text{K}$ . For weakly-bound molecules the trap depth is twice that for atoms (because the polarizability is that of two atoms), however, the trapping frequencies are the same for atoms and molecules, as the extra trap depth cancels out with the twice larger mass  $M$  of the molecule.

The extra Stark shift laser has a wavelength of  $\lambda = 1950 \text{ nm}$  and a maximum power of  $P = 1.7 \text{ W}$  at a waist of  $w = 125.9 \mu\text{m}$ . This provides an extra trap depth

$$U_v = \alpha_{x,v} P / (\pi w^2 c \epsilon_0) \quad (\text{S16})$$

between  $67.1 \text{ kHz} \times h$  and  $79.4 \text{ kHz} \times h$  per atom in the molecule and an extra radial confinement that varies from  $\Omega_v = 2\pi \times 44.1 \text{ Hz}$  to  $\Omega_v = 2\pi \times 48.0 \text{ Hz}$ . The polarizability per atom varies between  $\alpha_x = 210.1 \text{ a.u.}$  for the most weakly

bound state and  $\alpha_x = 248.5 \text{ a.u.}$  for the rovibrational ground state.

The temperature-independent shift  $\Delta U$  of up to  $12.3 \text{ kHz} \times h$  by far outweighs the temperature-dependent term. Note that the total shift for the diatomic molecule is  $2\Delta U$  and it therefore reaches  $24.6 \text{ kHz} \times h$ . The extra temperature-dependent term stems from the change in the total radial confinement of the effective trap created by the lattice and ac Stark laser. The contribution to radial trapping from the ac Stark laser is an order of magnitude smaller than the baseline provided by the lattice laser. The figure of merit is the difference in the extra confinement between different vibrational states as compared to the lattice radial frequency. We find  $\Delta\omega$  to vary between  $2\pi \times 6.4 \times 10^{-4} \text{ Hz}$  for a  $v = 61 \leftrightarrow v' = 62$  transition and  $2\pi \times 0.38 \text{ Hz}$  for a  $v = 0 \leftrightarrow v' = 62$  line. The total temperature-dependent shift,  $k_B T(\Delta\omega/\omega_r)$  is consistently below 0.7% of the temperature-independent shift, at most  $84.3 \text{ Hz} \times h$  for the  $v = 0 \leftrightarrow v' = 62$  transition. This is already significantly smaller than our experimental error bars.

We also point out that most of the thermal shift is, just like  $\Delta U$ , directly proportional to the differential polarizability we aim to measure. In fact, the linear term in the Taylor expansion for  $\Delta\omega$ , Eq. (S9) overestimates the real value by at most 0.4% making the nonlinear systematic negligible for this work.

Another possible source of systematic error is the variation in magic wavelength and the corresponding lattice radial confinement between the different molecular lines. We find that this variation contributes at most a 1.2% relative uncertainty to the temperature-dependent shift. Again, for us this contribution is two order of magnitude smaller than our experimental uncertainty and therefore negligible.

#### S4. UNCERTAINTY OF THE THEORETICAL POLARIZABILITIES DUE TO EMPIRICAL POTENTIAL

To calculate the blackbody radiation shifts we needed the vibrational wavefunctions for all nonrotating vibrational states of strontium molecules in their electronic ground state. These were obtained by solving the radial Schrödinger equation using an accurate potential obtained empirically from Fourier transform spectroscopy [S7]. The potential was provided in two versions: one in terms of a piecewise function and as a Morse/Long-Range (MLR) fit [S8]. We used the latter.

In the paper we estimated the uncertainty of the theoretical model by comparing theoretical ac polarizabilities to experimental data and concluded that model is accurate to within 2.6%. We expect that most of this error bar is coming from the combination of the limited accuracy of the *ab initio* polarizabilities and the experimental accuracy. Here, we additionally look at the uncertainty of the theoretical model stemming from the use of an empirical potential [S7]. To estimate the sensitivity of the theoretical polarizabilities to the experimental uncertainty we vary three of the most important parameters of the potential – dissociation energy  $D_e$ , equilibrium distance  $R_e$  and the leading van der Waals coefficient  $C_6$  and

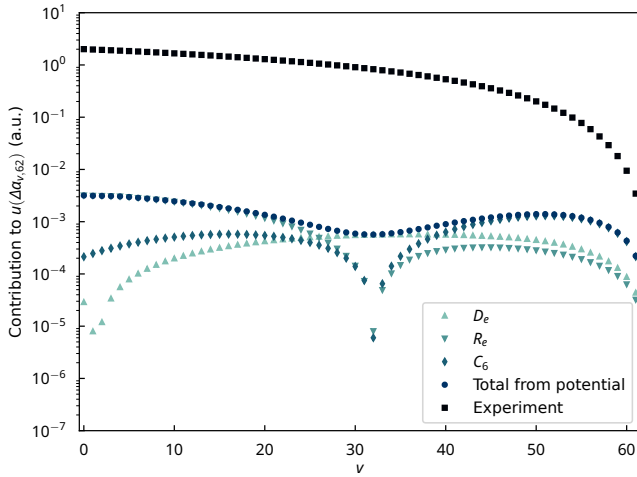


FIG. S3. Contributions to the uncertainty of the theoretical polarizabilities due to the use of empirical potential from Ref. [S7]. For all investigated transitions the contributions are all at least one order (typically more than two) of magnitude smaller than the error bar assigned to our theoretical model through comparison with experiment.

rerun our calculation. The parameters  $R_e = 4.6720(1)$  Å and  $D_e = 1081.64(2)$  cm<sup>-1</sup> [S7] are varied within their stated experimental uncertainties whereas  $C_6$  was varied such that the (well known) position of the near-threshold  $v = 62$  bound state at  $-137$  MHz shifted by at most 1 MHz.

The contributions to due to  $D_e$ ,  $R_e$  and  $C_6$  are shown in Fig. S3. The variation of each parameter influences the predicted polarizabilities in a distinct manner. As the polarizability depends chiefly on the mean internuclear distance of a given vibrational level, scaling the potential depth  $D_e$ , for example, has little influence on the polarizability of deeply bound states. On the other hand, these states are naturally more sensitive to varying the equilibrium distance  $R_e$ . Lastly, weakly bound states are the most sensitive to the variation of the long-range van der Waals interaction coefficient,  $C_6$ . Nevertheless, we find that all of these error contributions are at least one order of magnitude smaller than the uncertainty we assigned to the model via direct measurements of ac Stark shifts and for our purposes are negligible.

## S5. THE PLANCK INTEGRALS

Our calculation of the blackbody radiation shift relies on expanding the differential polarizability of a transition in terms of a series of Cauchy coefficients. Averaging each contribution to the polarizability over the Planck distribution involves calculating integrals of the following type:

$$c_n = \int_0^\infty \frac{u^{3+n}}{\exp(u)-1} du = \text{Li}_{n+4}(1)\Gamma(n+4) \quad (\text{S17})$$

for even  $n$ . Here  $\text{Li}_s(z)$  is the polylogarithm function of order  $s$ ,

$$\text{Li}_s(z) = \sum_{k=1}^{\infty} \frac{z^k}{k^s}, \quad (\text{S18})$$

and  $\Gamma(x)$  is Euler's gamma function. While for our purposes it was enough to cut the series off at  $n = 4$ , in the future higher orders might be needed. For future reference, here we list the first eight integrals:

$$\begin{aligned} c_0 &= \frac{\pi^4}{15} \approx 6.49393940226683 \dots \\ c_2 &= \frac{8\pi^6}{63} \approx 122.081167438134 \dots \\ c_4 &= \frac{8\pi^8}{15} \approx 5060.54987523764 \dots \\ c_6 &= \frac{128\pi^{10}}{33} \approx 363240.911422383 \dots \\ c_8 &= \frac{176896\pi^{12}}{4095} \approx 39926622.9877311 \dots \\ c_{10} &= \frac{2048\pi^{14}}{3} \approx 6227402193.41097 \dots \\ c_{12} &= \frac{3703808\pi^{16}}{255} \approx 1307694352218.91 \dots \\ c_{14} &= \frac{1437433856\pi^{18}}{3591} \approx 355688785859224. \quad (\text{S19}) \end{aligned}$$

\* These authors contributed equally to this work.

† mateusz@cold-molecules.com

‡ tanya.zelevinsky@columbia.edu

[S1] K. H. Leung, I. Majewska, H. Bekker, C.-H. Lee, E. Tiberi, S. S. Kondov, R. Moszynski, and T. Zelevinsky, Transition strength measurements to guide magic wavelength selection in optically trapped molecules, *Phys. Rev. Lett.* **125**, 153001 (2020).

[S2] K. H. Leung, B. Iritani, E. Tiberi, I. Majewska, M. Borkowski, R. Moszynski, and T. Zelevinsky, Terahertz vibrational molecular clock with systematic uncertainty at the 10<sup>-14</sup> level, *Phys. Rev. X* **13**, 011047 (2023).

[S3] M. S. Safronova, private communication (2023).

[S4] K. D. Bonin and V. V. Kresin, *Electric-dipole polarizabilities of atoms, molecules, and clusters* (World Scientific, 1997).

[S5] S. S. Kondov, C.-H. Lee, K. H. Leung, C. Liedl, I. Majewska, R. Moszynski, and T. Zelevinsky, Molecular lattice clock with long vibrational coherence, *Nature Physics* **15**, 1118 (2019).

[S6] L. Landau and E. Lifshitz, *Statistical Physics* (Pergamon Press, 1958).

[S7] A. Stein, H. Knöckel, and E. Tiemann, <sup>1</sup>S+<sup>1</sup>S asymptote of Sr<sub>2</sub> studied by Fourier-transform spectroscopy, *Eur. Phys. J. D* **57**, 171 (2010).

[S8] R. J. Le Roy, N. S. Dattani, J. A. Coxon, A. J. Ross, P. Crozet, and C. Linton, Accurate analytic potentials for Li<sub>2</sub>(X <sup>1</sup>Σ<sub>g</sub>) and Li<sub>2</sub>(A X <sup>1</sup>Σ<sub>u</sub><sup>+</sup>) from 2 to 90 Å, and the radiative lifetime of Li(2p), *The Journal of Chemical Physics* **131**, 204309 (2009).